Deep–Sea Research II 195 (2022) 105000

Contents lists available at ScienceDirect

Deep-Sea Research Part II

journal homepage: www.elsevier.com/locate/dsr2

The thermodynamic and dynamic control of the sensible heat polynya in the western Cosmonaut Sea

Zheng Wei, Zhaoru Zhang *, Xiaoqiao Wang, Yuanjie Chen, Meng Zhou

School of Oceanography, Shanghai Jiao Tong University, 1954 Huashan Road, Shanghai, 200030, China

ARTICLE INFO

Keywords:
West Cosmonaut Sea Polynya
Heat budget analysis
Dynamical processes
Cyclonic wind field

ABSTRACT

A prominent feature in the west Cosmonaut Sea is the reoccurrence of a sensible heat polynya — the western Cosmonaut Sea Polynya (wCSP), which normally exists in late austral autumn and early winter. The Southern Ocean Sate Estimate (SOSE) reanalysis product is employed to investigate the thermodynamic and dynamic processes controlling the formation and evolution of a real wCSP event in 2009, when the polynya properties revealed from satellite observations are reasonably simulated by SOSE. An oceanic heat budget analysis was conducted for the surface layer above the thermocline, and the results reveal that heat advection is the major term contributing to the surface heat content variation in this area. The precursor of wCSP — an embayment — was formed during cyclonic atmospheric circulations. The negative wind stress curl from a cyclone induced upwelling that brought the warm circumpolar deep water to the surface and presumably melted ice. Meanwhile, the location of the cyclone relative to the wCSP created weaker easterlies over the northern boundary of polynya and stronger easterlies over the southern boundary of polynya. This leads to difference in the meridional oceanic heat transports across the northern and southern boundaries, resulting in net positive meridional oceanic heat transport into the polynya. Both the vertical heat advection and the meridional heat advection contribute significantly to increased heat content in the surface layer of wCSP, causing sea-ice melt and formation of the embayment. The cyclonic wind field promotes convergence of sea ice over the northern area of the embayment and results in the polynya. The formation of wCSP is likely related to the strength and position of Southern Annular Mode on interannual scale, and may potentially affect the biological productivity by controlling the availability of light in the mixed layer.

1. Introduction

The Southern Ocean is largely covered by sea ice in austral autumn and winter, but there are also open water areas within the ice pack ranging in size from 10 to 10^5 km^2 which are called polynyas. By the mechanisms of formation and maintenance, polynyas can be categorized into two types: latent heat polynyas and sensible heat polynyas. The former normally occur along the Antarctic coasts and are formed and maintained by wind forcing and divergent ocean currents. The latter are formed and maintained mainly by the upwelled heat from depth which melts pre-existing sea ice and prevents the formation of new ice. Both polynyas are associated with convectional processes that may potentially affect atmosphere-ocean heat exchange (Morales Maqueda et al., 2004; Haid and Timmermann, 2013; Guo et al., 2019), the vertical nutrient and carbon fluxes (Arrigo et al., 1999; Hoppema and Anderson, 2007) and the thermohaline circulation.

There is a persistent sensible heat polynya observed in the western Cosmonaut Sea along the far eastern margin of the Weddell Gyre and offshore Enderby Land (Fig. 1), which has occurred almost every year based on satellite passive microwave observations available since the late 1970s. Comiso and Gordon (1987) first reported this polynya and named it the western Cosmonaut Sea Polynya (wCSP). Based on sea-ice concentration (SIC) data derived from the Scanning Multichannel Microwave Radiometer (SMMR) instrument on the Nimbus-7 satellite, they described the location, time of occurrence, behavior and duration of wCSP. The wCSP was formed in early winter and could last for few weeks. The interannual variability of the polynya size and persistence was substantial, and five remarkable polynya events were found from 1973 through 1986. Comiso and Gordon (1996) then analyzed the SIC data derived from the Special Sensor Microwave/Imager (SSM/I) and found that the wCSP became more active and had recurred several times during the winter from 1987 through 1993. They suspected that the

* Corresponding author.
E-mail address: zrzhang@sjtu.edu.cn (Z. Zhang).

https://doi.org/10.1016/j.dsr2.2021.105000
Received 15 May 2021; Received in revised form 13 November 2021; Accepted 15 November 2021
Available online 20 November 2021

more active polynya events were closely related to the changes in regional oceanic and atmospheric conditions. They also speculated that the oceanic convection would bring heat into the surface layer and cause the formation of the polynya, which was large enough to potentially impact the ventilation and the formation of the bottom water. Prasad et al. (2005) applied a coupled ocean-sea ice model to study the formation of wCSP from May to July of 1999. They changed the wind speed, wind direction and the sea-ice dynamic module in the model to study the roles of different physical processes responsible for the formation and maintenance of wCSP, which evolves from an embayment on the edge of the ice-covered area to a polynya. A numerical model study by Bailey et al. (2004) tested the sensitivity of the wCSP formation to atmospheric forcing, vertical heat fluxes and surface ocean currents, and showed that the wCSP formation was largely influenced by mesoscale atmospheric divergence events and can be maintained by vertical heat fluxes. Using sea-ice data from SMMR, Geddes and Moore (2007) calculated the time series of the embayment area and found that the area exhibited a three-year periodicity. This phenomenon indicates that heat in the surface ocean controlling the embayments and polynyas has periodic temporal variations, which may be associated with the cycle of the Antarctic Circumpolar Wave (White and Peterson, 1996). They also found that the large ice embayment events would be more likely to result in polynya formation, such as the embayment events that occurred in 1980 and 1999.

While earlier studies used idealized numerical experiments to investigate the effects of atmospheric and oceanic processes on the wCSP formation and characteristics, we utilized an ocean-sea ice reanalysis product to investigate the thermodynamical and dynamical factors controlling the formation and evolution of a real wCSP event during May to July of 2009, when the observed polynya characteristics are reasonably well captured by the Southern Ocean State Estimate (SOSE) simulations. SOSE is the only ocean-sea ice reanalysis product specifically targeted on the Southern Ocean, and the assimilation of large amount of observational data in SOSE produces more realistic simulations of Southern Ocean oceanic processes. In particular, a heat budget analysis is performed to quantify the roles of different heat budget terms in the realistic formation and evolution of the embayment — the precursor of wCSP, and oceanic and atmospheric processes modulating the temporal variations of crucial heat budget terms are analyzed to reveal the dynamical and thermodynamical control mechanisms on the formation of wCSP. In addition to the role of atmospheric forcing and vertical heat fluxes as revealed from previous work, this study demonstrates that meridional heat fluxes are also important in creating and maintaining the polynya.

2. Data and methods

2.1. The reanalysis product

The oceanic and atmospheric variables used in this study are from the SOSE, which is the only reanalysis product targeting on the Southern Ocean. The ocean-sea ice model used in SOSE is an evolved version of the Massachusetts Institute of Technology General Circulation Model (MITgcm), which assimilates observational data including potential temperature, practical salinity and velocity fields (Mazloff et al., 2010). SOSE employs an adjoint method for data assimilation, which applies more dynamically consistent constraints for different oceanic variables. The horizontal resolution of the model is $1/6^\circ \times 1/6^\circ$. The model has 42 vertical levels and the vertical resolution is enhanced in surface layers. The atmospheric forcing of SOSE in 2009 comes from the European Centre for Medium-Range Weather Forecasts (ECMWF) Reanalysis Interim (ERA-Interim) product. The initial and northern boundary conditions come from the OCean Comprehensible Atlas (OCCA) global state estimate (Forget, 2010).

The thermodynamic sea ice module of SOSE is based on the work of Semtner (1976), who applied one-dimensional heat diffusion process to sea ice and modified it to include the influence of solar radiation penetration, internal brine rejection and snow cover insulation. This module has been used to study the relationship of variability between the sea ice and ocean (Fenty and Heimbach, 2013). The dynamic sea ice module in SOSE is derived from Hibler and Bryan (1979), which employed nonlinear plastic rheology and considered the effects of ice deformation and thickness on the internal stresses in the ice cover. The advection scheme for sea-ice thickness equations in the model employs a modified Euler step (Kurihara, 1965), which applies second-order-accurate discretization in time. Previous studies have employed SOSE to study Antarctic coastal polynyas and water mass transformations (Abernathey et al., 2016), which suggests that SOSE can reasonably simulate the coupled ocean-sea ice processes within polynyas.

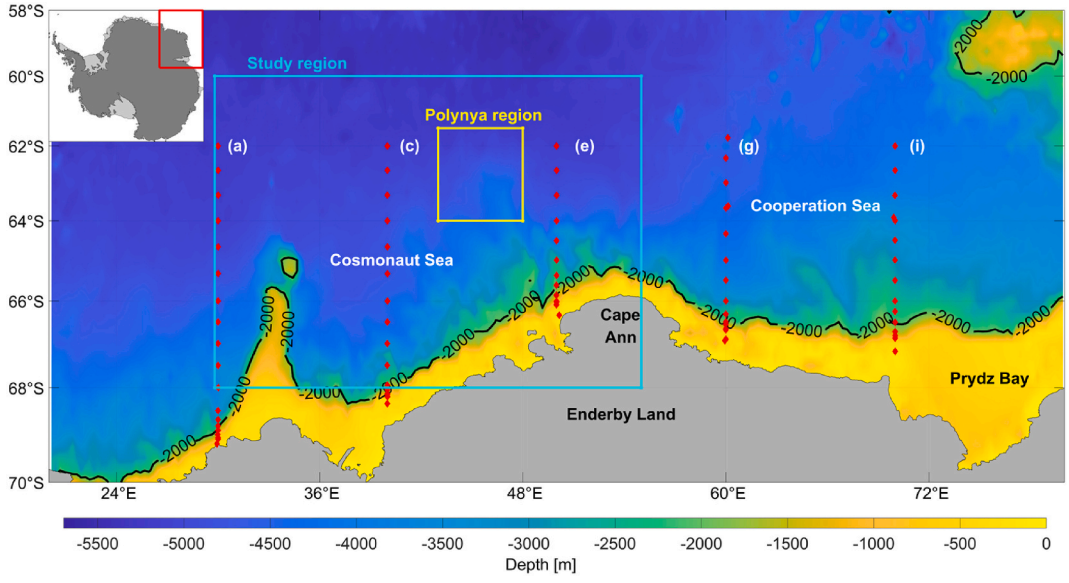

Fig. 1. The bathymetry (m) of the Cosmonaut Sea, the adjacent Cooperation Sea and the Prydz Bay. Red diamonds indicate the observation transects (a, c, e, g and i) during the Baseline Research on Oceanography, Krill and the Environment-West (BROKE-West) survey in 2006. The study region and polynya region are marked by cyan and yellow boxes, respectively. The 2000-m isobath is indicated by the black line.

2.2. Validation of the SOSE simulations

2.2.1. Sea ice

To verify whether the SOSE simulations can capture the observed sea-ice properties, in particular their temporal variations in the wCSP area, the SIC dataset derived from Advanced Microwave Scanning Radiometer-Earth Observing System sensor (AMSR-E) is used to validate the ice concentration simulations from SOSE. The horizontal resolution of AMSR-E is 12.5 × 12.5 km. Maps of five-day averaged SIC from AMSR-E and from SOSE during the polynya formation seasons, i.e., from May to August of 2009 are well captured, including the process from the formation of an embayment (June 29) to the formation of a polynya (July 4) (Figs. 2 and 3). Moreover, the location and extent of the embayment and polynya are relatively consistent with observations, though the duration of the polynya is shorter in SOSE compared to that in observations that lasted until July 19. The locations of wCSP in both AMSR-E and SOSE varied slightly from year to year, and a minimum area enclosing all locations of the polynya over 2005–2010 (30–55°E, 68–60°S) is selected as our study region. Area-averaged SIC over the study region from May to July and over the polynya region (43–48°E, 64–61.5°S) covering the polynya-existence period indicates that the SOSE simulation overestimates SIC compared to the AMSR-E observations (Fig. 4), but the correlation coefficient (R) between SOSE and AMSR-E is 0.96 ($P < 0.0001$). For the polynya region before June 14, SIC from SOSE and AMSR-E are consistent. After June 14, the SOSE simulation overestimates SIC, but the temporal variation of the SOSE SIC is significantly correlated with that from AMSR-E ($R = 0.93$, $P < 0.0001$). The general consistency in the evolution of SIC from SOSE and AMSR-E suggests that it is reasonable to use the SOSE simulations for investigating the mechanisms controlling the formation and variation of key sea-ice features, including polynyas and embayments.

2.2.2. Ocean temperature

Observations of oceanic quantities are rare in winter; therefore, we used summer observations to assess the performance of SOSE in simulating the ocean temperature. The observational data come from the Seabird SBE-911 CTD (Conductivity, Temperature, Depth) measurements during the Baseline Research on Oceanography, Krill and the Environment-West (BROKE-West) survey period, which covered the Cosmonaut Sea and the Cooperation Sea from January to March 2006 (Fig. 1). Comparisons between the potential temperature from SOSE and observations (Fig. 5) show that in summer intense shortwave radiation keeps the ocean surface layer warm, reaching as high as 1 °C based on observations. The subsurface cold water mass, which is the winter water, is located at 20–100 m, and extends as far south as 68°S along the 30°E section (Fig. 5a). Circumpolar deep water (CDW) lies under the winter water and extends southward as far as the continental slope. There is a westward Antarctic slope current, which establishes a front separating the cold and fresh shelf water (SW) from the warm and saline CDW offshore. Although the SOSE simulation overestimates the surface water temperature, the distributions of the three water masses in SOSE show overall agreement to those in observations. It should be noted that although there are no winter observational data available to validate the SOSE performance, given the fact that sea-ice data are not assimilated into SOSE (Mazloff et al., 2010), the good performance of SOSE in simulating the winter SIC indicates that the thermodynamical processes in the surface ocean in this season are well simulated by SOSE.

2.3. Heat budget analysis

To reveal the thermodynamic controlling mechanisms for the formation of the embayment and the polynya, heat budget analysis is performed for the layer above the thermocline in the study area based on the SOSE product. The 5-day-average output of heat budget terms from the SOSE simulation are used, which guarantees that the heat budget equation is closed. The thermocline is determined based on the SOSE simulated density profiles and occurs around 70 m, which is approximately the interface between the winter water and CDW. As this study relies on the SOSE product for the heat budget analysis, for consistency the region selected for calculations of different heat terms covers the polynya area simulated by SOSE (Fig. 3m). We defined a surface box in the wCSP area separated from the subsurface layers at this depth (the lateral extent of the box is indicated by the black rectangle in Fig. 3m). The temporal variation of potential temperature is computed by:

$$\theta_t = -u\theta_x - v\theta_y - w\theta_z + \nabla\cdot k\nabla\theta + \nabla^2\cdot k_2\nabla^2\theta + D_{kpp} + D_i + F_{atmosphere} + F_{ice} \quad (1)$$

where θ is potential temperature; θ_t is the tendency term that represents the net heat change; $-u\theta_x$, $-v\theta_y$ and $-w\theta_z$ are the zonal advection,

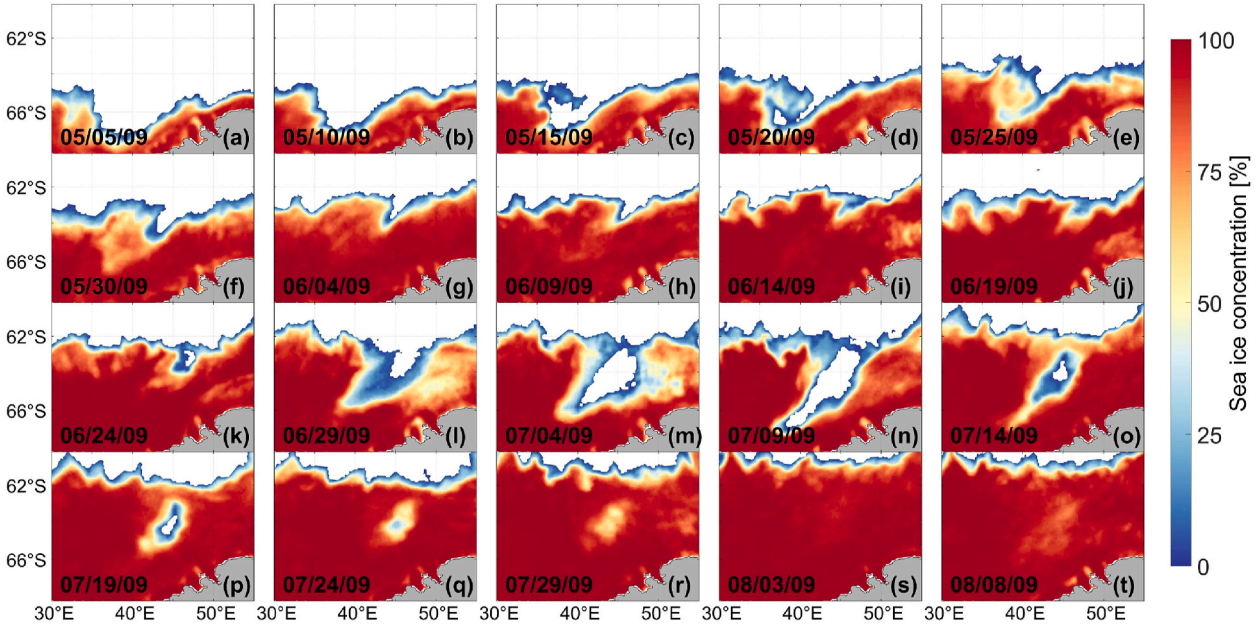

Fig. 2. Maps of five-day averaged SIC from AMSR-E from 5 May 2009 to 8 August 2009.

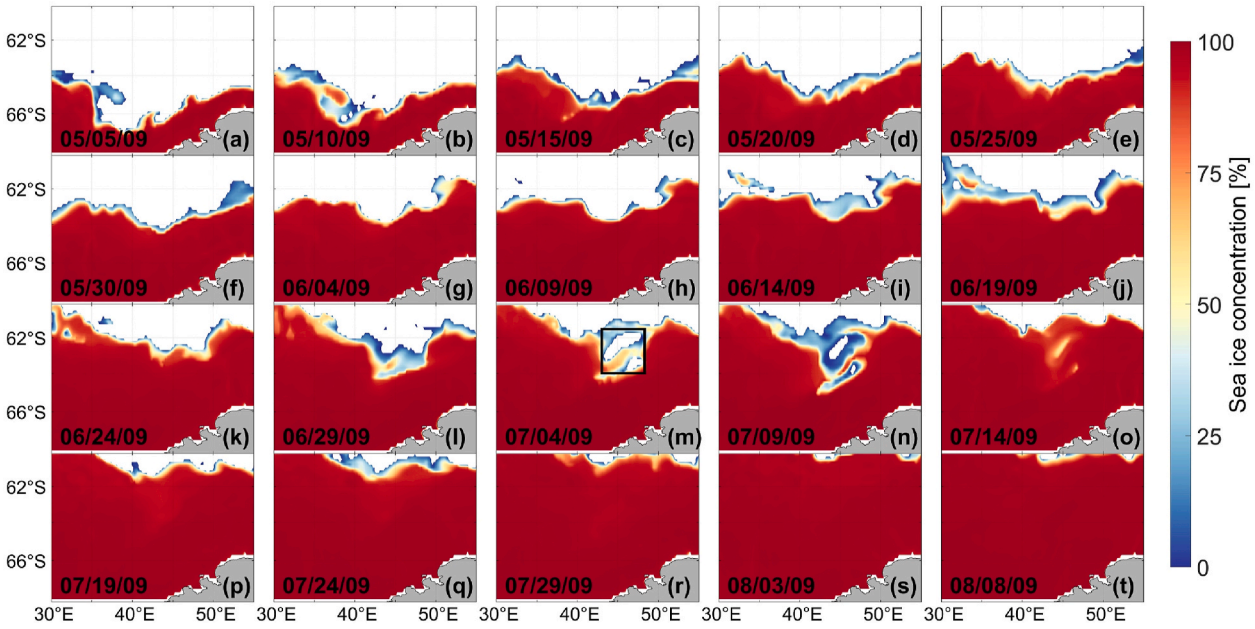

Fig. 3. Maps of five-day averaged SIC from SOSE from 5 May 2009 to 8 August 2009. The polynya region is labeled by the black box in (m).

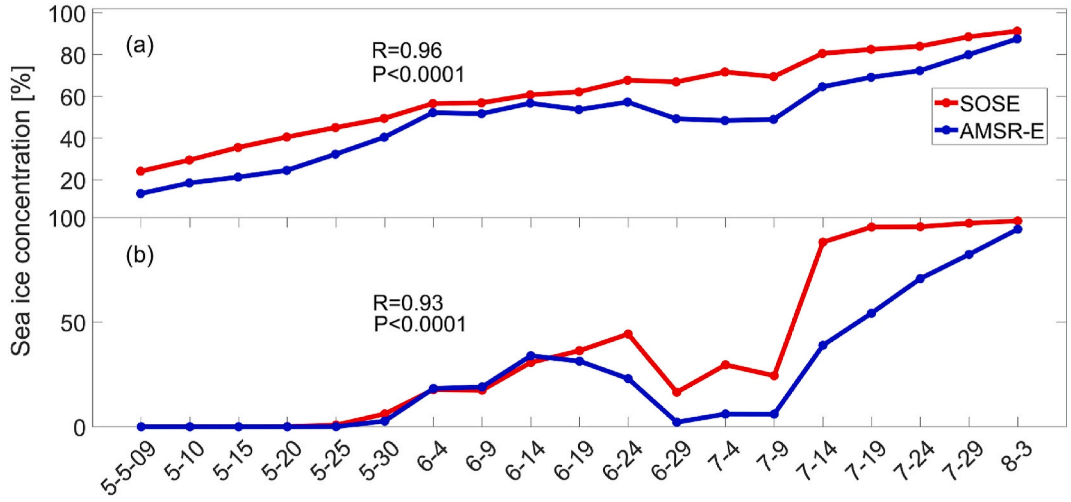

Fig. 4. Time series of five-day averaged SIC from SOSE and AMSR-E over (a) the study region (30–55°E, 68–60°S) and (b) the polynya region (43–48°E, 64–61.5°S) from 5 May 2009 to 3 August 2009.

meridional advection and vertical advection terms; k and k_2 are the harmonic and biharmonic diffusion coefficients, and the mixed-layer turbulence is parameterized as D_{kpp} by the K-Profile Parameterization (KPP). D_i represents the implicit diffusion term, $F_{atmosphere}$ represents the net heat fluxes between the ocean and atmosphere, and F_{ice} represents the net heat fluxes between ocean and sea ice. The harmonic, biharmonic, parameterized, and implicit diffusion terms can be grouped into one diffusion term (D), and the atmospheric and sea-ice forcing terms can be grouped into one forcing term (F). We approximate the heat budget by integrating equation (1) over the wCSP and multiplying it by the specific heat capacity ($C_v = 3985$ J kg^{-1} °C^{-1}) and reference sea water density $\rho_0 = 1035$ kg m^{-3}.

3. Results

3.1. Heat budget in the surface layer of the polynya area

Previous works analyzing long time-series data of polynya properties normally obtain anomaly time series of variables to study their high-frequency (below the seasonal scale) variations (Ding et al., 2020; Lei et al., 2020). In our study the formation and duration of the wCSP only spanned one to two months, which do not include low-frequency signals that need to be removed, and thus the original time series of sea ice and oceanic variables are used. A time series of five-day averaged heat budget terms over the polynya area from May to July of 2009 (Fig. 6a) indicated that the diffusion term was relatively small compared with the other three terms and thus can be neglected. The advection term represents the heat transported by ocean currents and was almost always positive, while the forcing term was always negative, which represents the heat persistently released from the ocean to the atmosphere and sea ice. The tendency term was mainly balanced between the advection term and the forcing term. Before June 9, the temporal variation of the tendency term was closely correlated with the temporal variation of the forcing term ($R = 0.99$, $P < 0.0001$), and the advection term was small. From June 9 to July 14, which covered the existence periods of the embayment and the wCSP (shaded region in Fig. 7), the tendency term

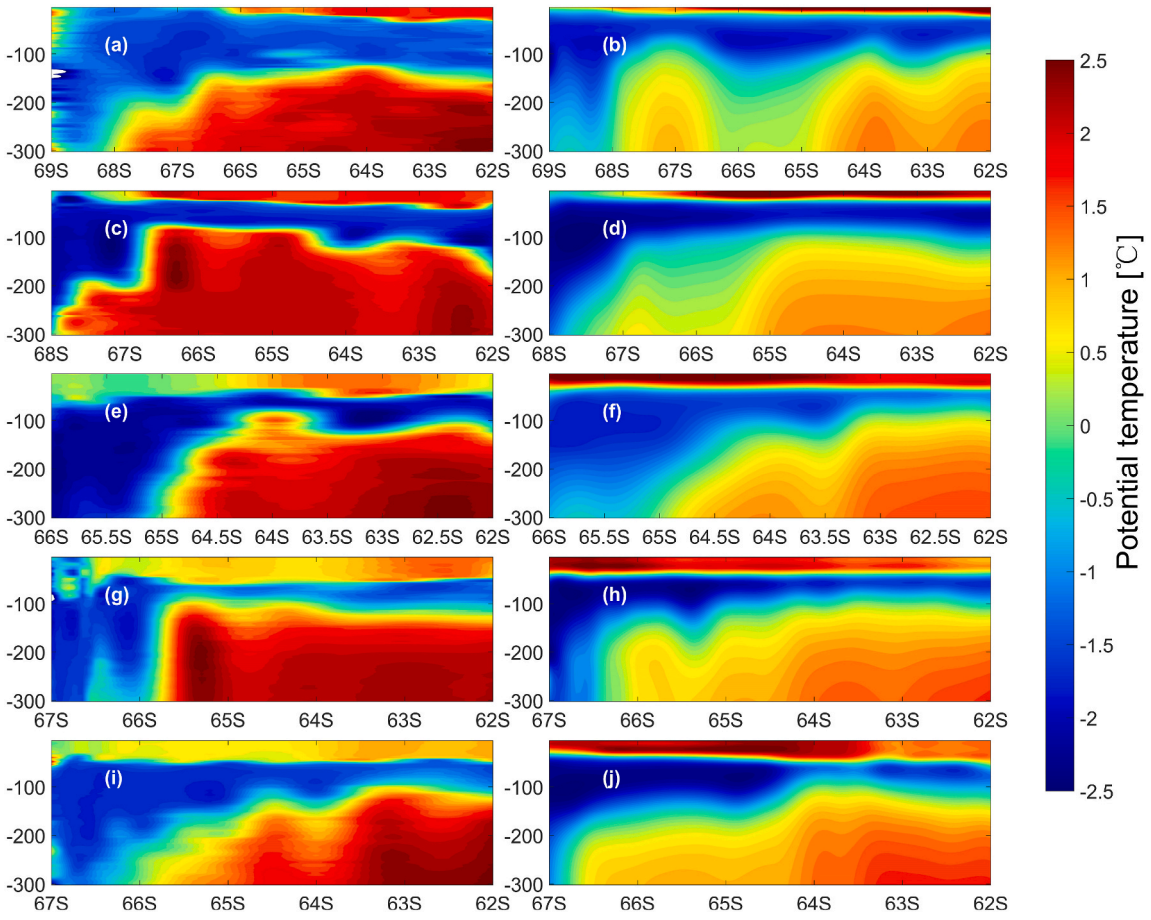

Fig. 5. Comparison between the vertical profiles of potential temperature along the cross-shore transects (Fig. 1) in the Cosmonaut Sea and Cooperation Sea from (a, c, e, g and i) the BROKE-West observations and (b, d, f, h and j) from SOSE.

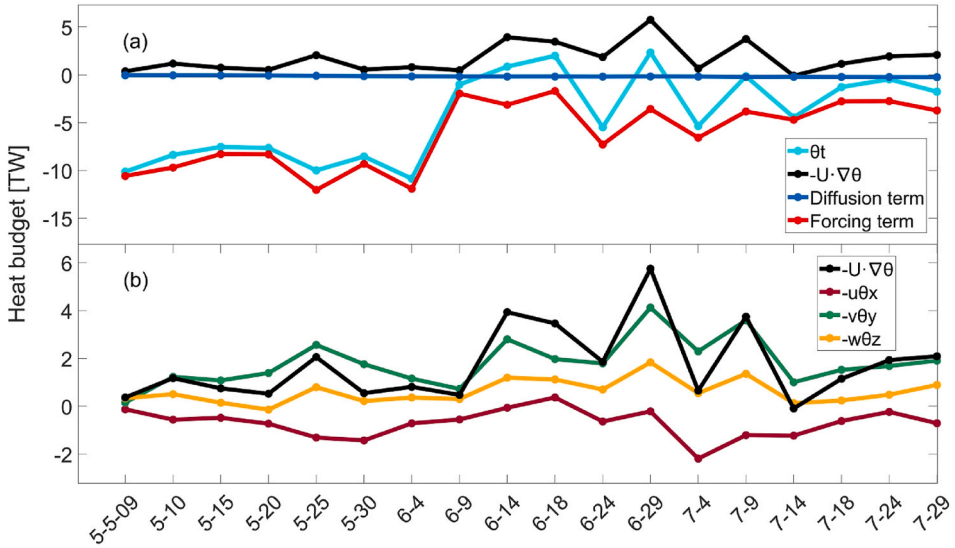

Fig. 6. (a) Time series of different terms in the heat budget equation in the period of May–July of 2009 that covers the formation period of the embayment and the polynya. (b) Time series of the zonal advection term ($-u\theta_x$), meridional advection term ($-v\theta_y$) and vertical advection term ($-w\theta_z$) in the same period. The advection term ($-\boldsymbol{U}\cdot\nabla\theta$) in Fig. 6a is the sum of advection components in Fig. 6b ($-\boldsymbol{U}\cdot\nabla\theta$).

was correlated both with the forcing term and the advection term, the correlation coefficients being 0.83 and 0.79 with the former and the latter, respectively. This suggests that the advective heat flux plays an important role in creating the embayment and polynya that normally appear in late May through June (Comiso and Gordon, 1996; Geddes and Moore, 2007).

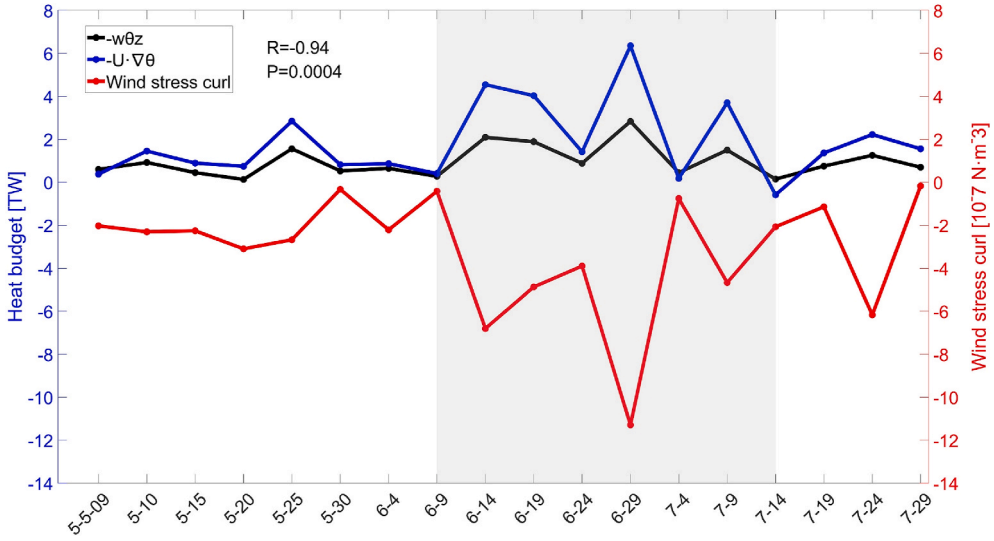

Fig. 7. Time series of the vertical advection term, the advection term and the wind stress curl. The correlation coefficient between the vertical advection term and the wind stress curl from June 9 to July 14 (shaded region) is provided.

3.2. Thermodynamical processes controlling the formation and maintenance of the embayment

On June 29 the advection term reached its maxima in May to June, which also resulted in a peak value in the tendency term. This is the date when the embayment — the precursor of wCSP — became apparent in both the SOSE simulation (Fig. 3l) and observations (Fig. 2l). This indicates that the rapid increase in the upper ocean heat by advection will melt pre-existing sea ice and lead to the decrease of SIC at the northern edge of the ice-covered area, forming the embayment. Similar peaks in the advection and tendency terms appeared on May 25 and June 14 when reduced SIC is observed along the ice edge but no embayment is formed; on these dates the advection and tendency terms were weaker than those on June 29. The polynya would persist for 10 days or more after being formed, and during this period, both of the vertical and meridional advection terms remained positive, indicating that they were the main heat sources for the persistence of the polynya. On July 9 (Fig. 3n), the advection term in the study region reached another peak, which caused the persistence of the low SIC until July 14.

The advection term is then decomposed into the zonal, meridional and vertical terms (Fig. 6b). The advection term was correlated with both the meridional advection term and the vertical advection term from June 9 to July 14, with the correlation coefficients being 0.87 ($P < 0.0001$) and 0.99 ($P < 0.0001$). The zonal advection term was almost always negative in this period, which demonstrates that there was persistent heat loss caused by the zonal flow. The meridional advection term was closely correlated with the vertical advection term ($R = 0.85$ and $P < 0.0001$). On June 29, the meridional advection term and the vertical advection term both became maximal.

The features of the advection terms were likely due to the variation of the wind field. Previous numerical studies revealed that mesoscale atmospheric divergence events, such as cyclones, would lead to the formation of the sensible polynya (Hirabara et al., 2012; Francis et al., 2019). The divergent wind field causes ice to diverge over the polynya and brings heat from below the thermocline into the upper ocean via Ekman pumping, which is sufficient to melt the reduced ice cover and open the polynya (Arbetter et al., 2004). For the wCSP, we calculated the time series of the area-averaged wind stress curl over the polynya region (43–48°E, 64–61.5°S) (Fig. 7). The value of the wind stress curl within the study period was always negative, which indicates that atmosphere circulation over the polynya was cyclonic. From June 9 to July 14, the wind stress curl was closely correlated with both the advection and vertical advection terms ($R = -0.92$, $P = 0.001$; $R = -0.94$, $P = 0.0004$). On June 29, strong upwelling events occurred over the polynya region (63.8–61.8°S; Fig. 8), which corresponded to the minima of the wind stress curl (Fig. 7) associated with a cyclonic atmosphere circulation (Fig. 9e). On June 14 and July 9, two weaker upwelling events occurred (Fig. 8b and g) following two minima of the wind stress curl. The upwelling areas corresponded exactly to the location where the wCSP was formed on July 4 (63.8–61.8°S).

This analysis reveals that the change in the heat content of the surface layer over the wCSP is mainly caused by oceanic heat advection. To quantify the relative importance of heat advection from different directions for the heat content variation in the wCSP area, the net heat transport across each boundary of the defined wCSP surface box is calculated, and the sum of heat transports across the western and eastern boundaries (zonal heat transport) and across the northern and southern boundaries (meridional heat transport) obtained (Fig. 10). The zonal heat transport was mostly negative for the wCSP area and was not significantly correlated with the net advection term. In contrast, the meridional heat transport was mostly positive over the study period, and was highly correlated with the net advection term ($R = 0.88$, $P < 0.001$). This demonstrates that in addition to the vertical heat advection, the meridional heat advection is also a primary modulator of the net heat advection and an important contributor to the ultimate heat change in the surface layer of wCSP. On June 29 there was a sudden increase in the meridional heat transport, resembling the variations in the net heat advection and the vertical heat advection. The increase in the meridional heat transport was related to the increase in the north-south gradient of the meridional velocity. The processes are as follows: The presence of the cyclone north of the wCSP (Fig. 9e) resulted in weak easterlies over the northern polynya boundary and strong easterlies over the southern boundary, which created weaker southward Ekman flow over the northern boundary and stronger southward Ekman flow over the southern boundary (Fig. 11e). The stronger meridional gradient in v enhanced the difference between the meridional heat transports ($v\theta_y$) across the two boundaries. The horizontal divergence generated by the difference in v between the northern and southern boundaries ($v_N - v_S$) promotes upwelling. $v_N - v_S$ are then computed (Fig. 10b), which shows significant and high correlation with the meridional heat transport, demonstrating the role of change in the meridional velocity contrast between the two boundaries in the temporal variation of the meridional heat advection term.

Upwelling events occurred over the polynya on 29 June 2009

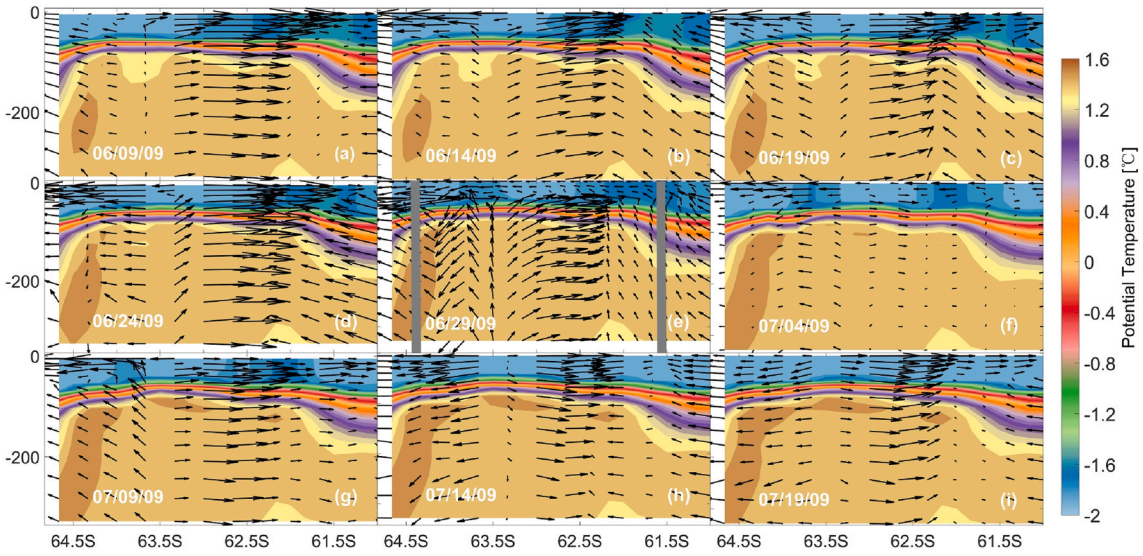

Fig. 8. Profiles of potential temperature profiles along 46°E from 9 June 2009 to 19 July 2009 in the polynya region. The flow fields are indicated by black arrows. The northern and southern boundaries of the wCSP are indicated by the grey bars in (e).

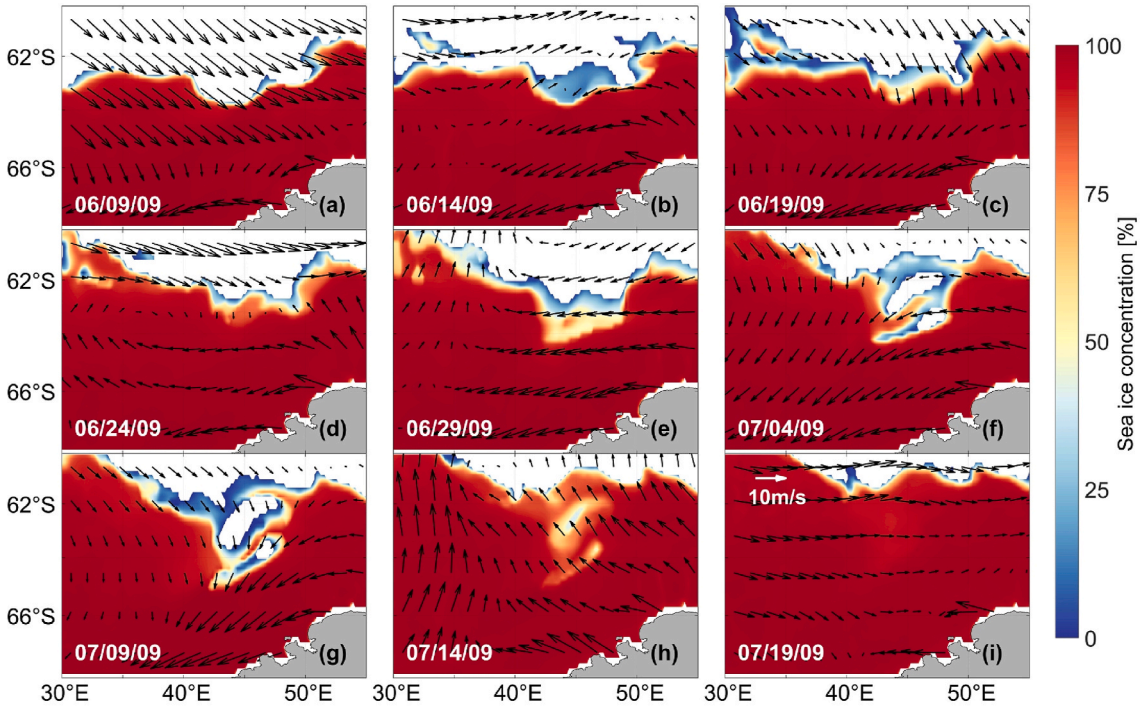

Fig. 9. Maps of five-day averaged SIC (colors) and wind field (vectors) from SOSE during 9 June 2009 through 19 July 2009.

(Fig. 8), associated with the negative wind stress curl induced by the cyclonic circulation. In addition to heat, the upwelling also brought salt from CDW and resulted in an increase in the surface salinity and potential density (Fig. 12). The increase in density will break stratification and favor the vertical flux of heat into the surface layer. The vertical and meridional heat advection, which were positive and increased from July 4 to July 9, together with the heat reservoir in the surface ocean all contributed to maintaining the polynya during this period (Fig. 8f and g). On July 10 the polynya and the surrounding area were influenced by southerlies (Fig. 13l), which transported sea ice from densely-distributed ice area to the polynya and drove the closure of the polynya.

3.3. Dynamical processes controlling the formation and closure of the polynya

On July 4, the heat tendency term showed a reduction relative to that on June 29 (Fig. 6a), and the heat tendency term changed from positive to negative, which indicated that the oceanic heat supply was not large enough to balance the surface heat loss to the atmosphere. This led to a decrease in ice concentration in the center of the polynya from June 29 to July 4. To understand the evolution from embayment to polynya, we examined the daily SIC and wind stress fields (Fig. 13). The polynya shape was initially formed on July 1 when the cyclone north of the polynya moved eastward, leaving the edge of its western branch over the polynya. As such, the eastern boundary of the embayment was impacted

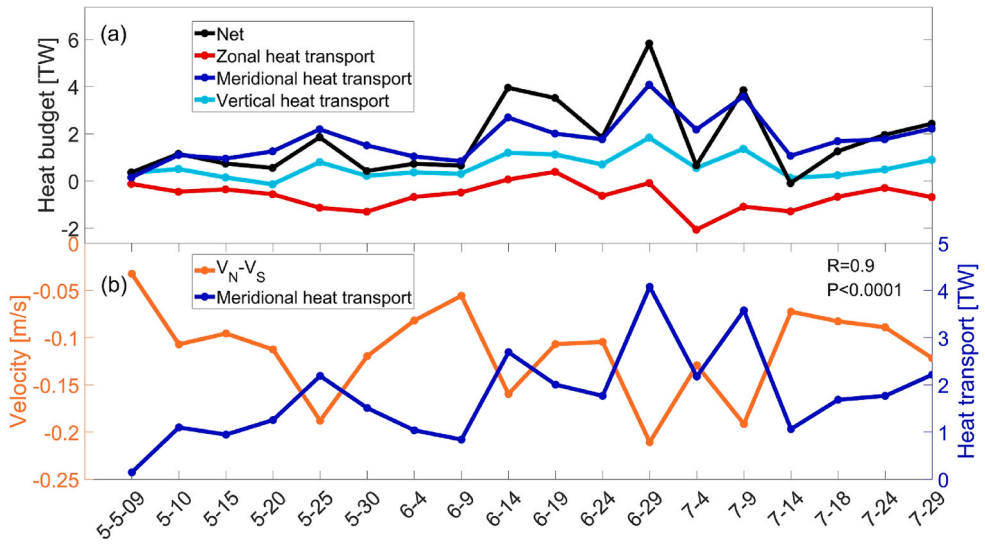

Fig. 10. (a) Time series of the net heat advection, the sum of heat transports across the eastern and western boundaries (zonal heat transport), the sum of heat transports across the northern and southern boundaries (meridional heat transport), and the vertical heat transport across the lower boundary of the surface box (Fig. 3m) over the wCSP area during the study period. (b) Time series of the difference between mean meridional velocity across the northern and southern boundaries ($v_N - v_S$) and the meridional heat transport.

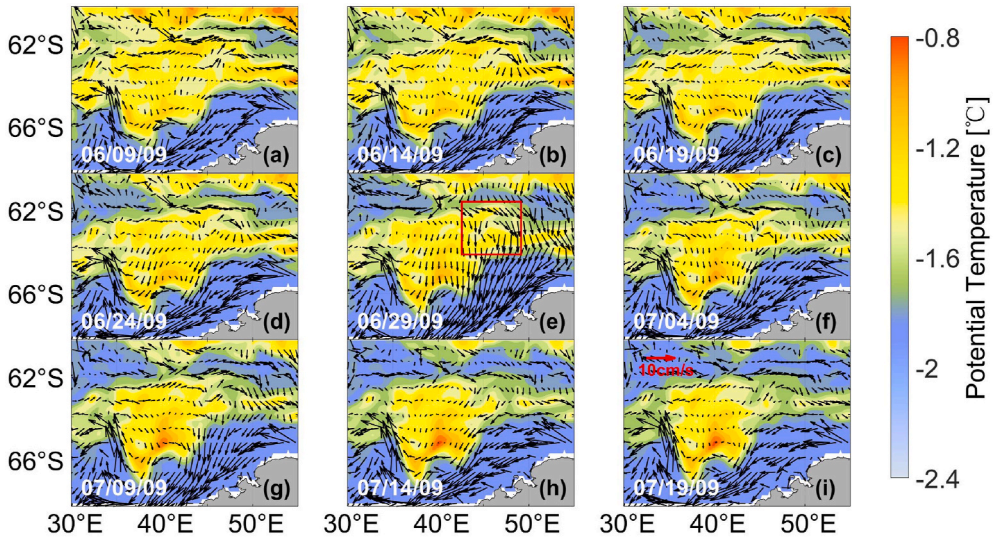

Fig. 11. Maps of the depth-averaged potential temperature (colors) and velocity field (vectors) above the thermocline from 9 June 2009 to 19 July 2009. The polynya region is labeled by the red box in (e).

by stronger southerly winds, which created stronger westward ice flow by Ekman transport compared to the weaker westward ice flow prevented by the compact sea ice near the western boundary. Such differential ice flow resulted in net transport of sea ice into the northern area of the embayment and resulted in sea-ice convergence, which formed the northern boundary of an enclosed polynya.

4. Discussion

4.1. Potential impacts of the wCSP on primary production

Biological productivity in the Southern Ocean is limited by irradiance and dissolved iron concentrations (De Baar et al., 2005; Boyd et al., 2007). It has been found that chlorophyll-a (Chl-a) concentrations in the Maud Rise Polynya is higher than that in the surrounding region in austral spring (Berg et al., 2020), which is caused by the improved irradiance environment and supply of iron through upwelling (Jena and Pillai, 2020). The difference from the Maud Rise Polynya is that the wCSP mainly exists in winter, and thus cannot directly affect the spring phytoplankton production. Compared with areas covered by thick ice, surface waters in coastal polynyas in winter are covered by thinner ice, which is melted and exposed to solar radiation earlier than other areas in spring, allowing light to penetrate into the ocean, and as such the polynya region can be more productive than the surrounding areas (Mundy and Barber, 2001).

To find out the potential impacts of wCSP on spring phytoplankton biomass, we analyzed the surface Chl-a data from the Moderate Resolution Imaging Spectroradiometer (MODIS) product on board the Aqua satellite and SIC data from the SMMR on board the Nimbus-7 satellite, which has longer time span than AMSR-E. Although *in situ* observations and ocean-color satellite observations in the Cosmonaut Sea in austral autumn are limited due to the weather and sea ice, we found that higher Chl-a values occurred in the wCSP region compared with the surrounding areas in 2003, 2016 and 2019, the years with a larger coverage of springtime Chl-a satellite data. The areas of high Chl-a concentrations in the western Cosmonaut Sea in the spring of 2003 (Fig. 14a), 2016 (Fig. 14d) and 2019 (Fig. 14g) generally corresponded with the regions where the embayment and polynya appeared in the preceding winter (Fig. 14b, e and h). In 2003, the region of higher Chl-a in spring was located more to the east relative to the wCSP and co-located with the

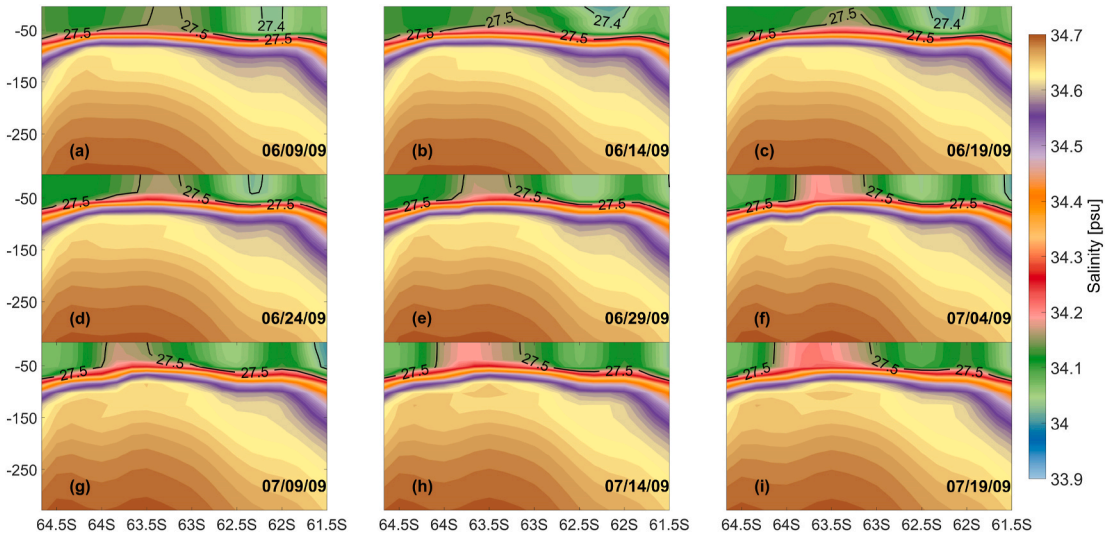

Fig. 12. Salinity profiles along 46°E from 9 June 2009 to 19 July 2009 in the wCSP region. Potential density anomaly contours are indicated by the black lines. The northern and southern boundaries of the wCSP are indicated by the red lines in Fig. 11e.

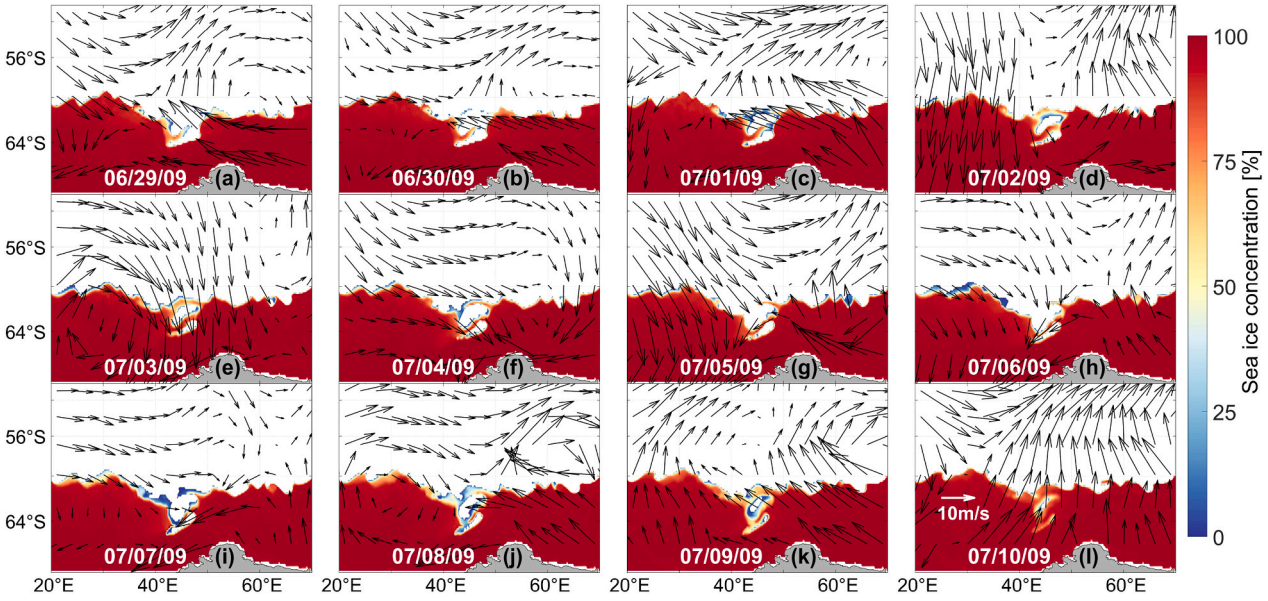

Fig. 13. Daily-averaged SIC (colors) and wind (vectors) fields from June 29 to July 10 over the wCSP formation period.

area where the sea ice firstly melted in spring (November 27) (Fig. 14c). The early melting of sea ice may result from thinner ice resulting from the wCSP formation and existence. In the spring of 2016 and 2019, there was fairly good correspondence between the areas of high Chl-a concentration and the wCSP locations, suggesting a close relationship between the winter existence of polynya and spring phytoplankton growth. The robustness of such relationship needs to be verified by additional satellite Chl-a data.

4.2. A possible link between the wCSP and Southern Annular Mode (SAM)

SAM, the dominant mode for controlling the climate change of Southern Hemisphere extratropical regions on seasonal to decadal scales, has significant effects on sea-ice processes in the Southern Ocean (Simpkins and Karpechko, 2011; Gille et al., 2016). The shift of SAM towards the positive phase will lead to an increase in the strength of the westerlies and a southward shift of its principal axis (Marshall, 2003; Sen Gupta and England, 2006). Uotila et al. (2013) showed that the frequency of cyclones in the Southern Ocean is closely associated with SAM, with increasing density of cyclones under a positive SAM phase. To explore the potential linkage of SAM to the cyclones in the western Cosmonaut Sea and thus to the formation of wCSP, we analyzed the 10-m wind stress curl field over our study area, which is obtained from the atmospheric reanalysis product ERA5 produced by the ECMWF (Hersbach et al., 2020). Time-series of the winter-mean wind stress curl over the region (30–55°E, 68–60°S) and the SAM index (Marshall, 2003) over 2006–2020 showed that the wind stress curl and SAM are significantly and negatively correlated (Fig. 15) ($R = -0.59$, $P = 0.005$). The correlation is higher during 2007–2013 ($R = -0.86$, $P = 0.01$), which suggests that more cyclones appear during the positive SAM phase. Several studies have investigated the relationship between the Weddell Polynya formation and the wind stress curl caused by SAM (Gordon et al., 2007; Cheon et al., 2014; Gordon, 2014; Campbell et al., 2019); the wind stress in this case results from the large-scale wind field generated by the westerlies and polar easterlies, while in the Cosmonaut

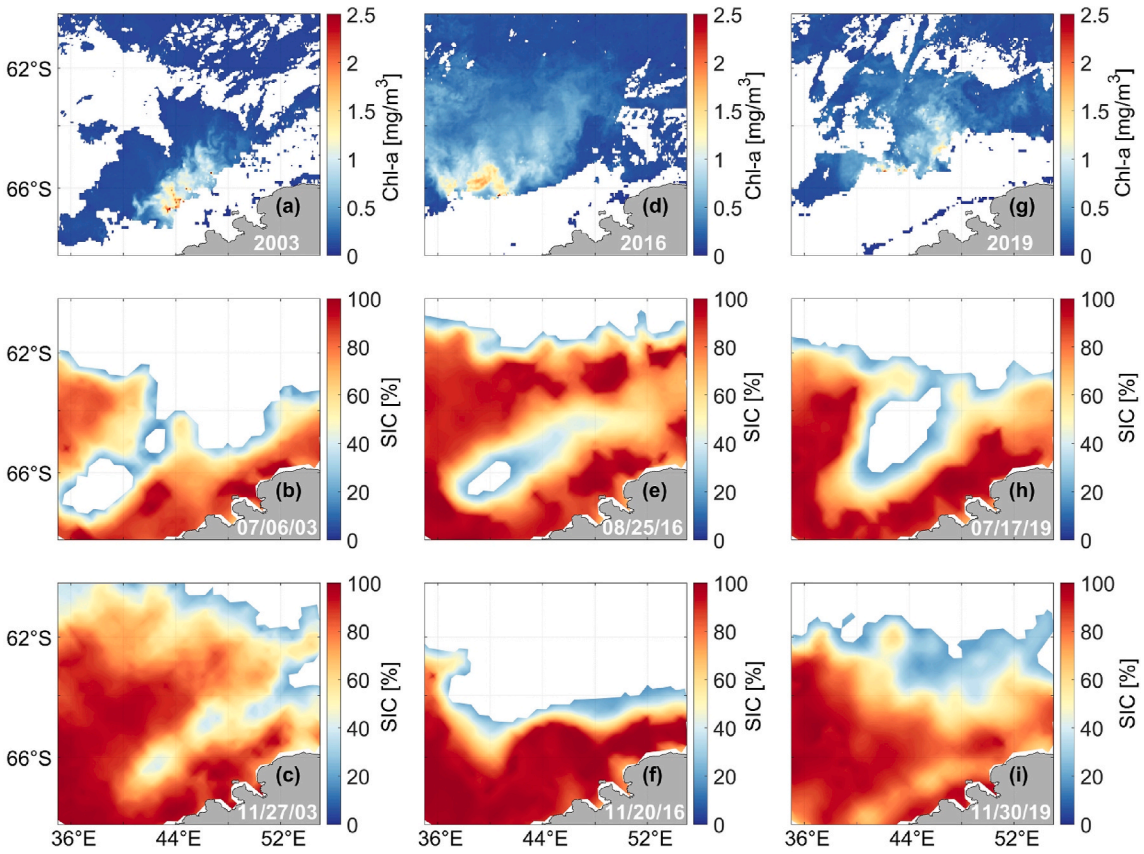

Fig. 14. (a), (d) and (g): Chl-a concentrations from MODIS in the spring of 2003, 2016 and 2019. (b), (e) and (h) show the locations of the wCSP in 2003, 2016 and 2019, respectively. (c), (f) and (i) show the SIC distributions in the spring of 2003, 2016 and 2019, respectively.

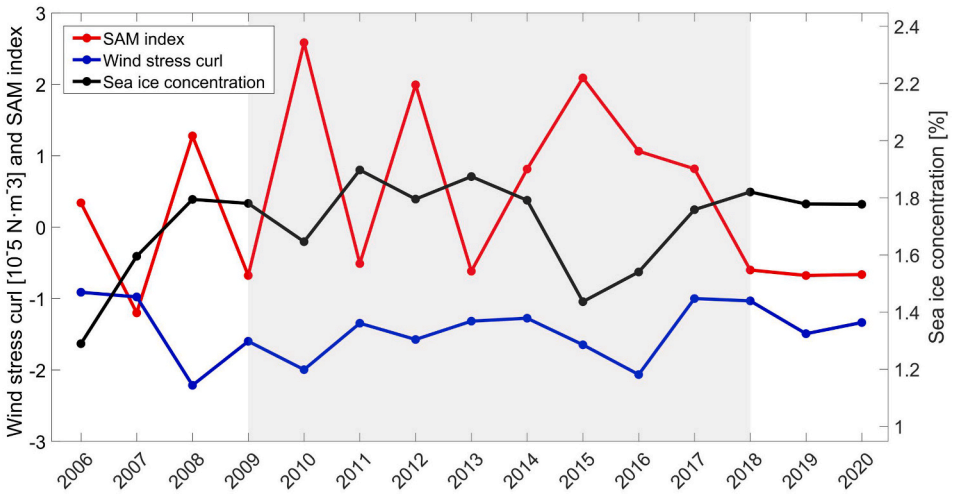

Fig. 15. Time series of the SAM index, winter-mean wind stress curl averaged over the study region (30–55°E, 68–60°S) and winter-mean SIC averaged over the wCSP region (40–48°E, 66–62°S). The correlation coefficient (R) between the SAM index and SIC from 2009 to 2018 (shaded region) is −0.67 (P = 0.03). R between the SAM index and the wind stress curl from 2009 to 2018 is −0.72 (P = 0.02), and R between SIC and the wind stress curl from 2009 to 2018 (shaded region) is 0.69 (P = 0.03).

Sea the wind stress curl results from the synoptic-scale cyclones.

The linkage between SAM and cyclones in our study area indicates a possible relationship between SAM and the formation of wCSP. To explore such relationship, we analyzed the winter-mean SMMR SIC data from 2006 to 2020 averaged over the region normally enclosing the wCSP formation site (40–48°E, 66–62°S), the winter-mean wind stress curl and the SAM index (Fig. 15). From 2009 to 2018, the significant negative correlation (R = −0.67, P = 0.03) between SIC and SAM, together with the positive correlation (R = 0.69, P = 0.03) between SIC and the wind stress curl, indicates that when SAM shifts to its positive phase, the increased density of cyclones passing the wCSP created more polynya events and resulted in a decrease in the SIC over the polynya. Prior to 2009 when the polynya formation was less active (not shown), there was no significant correlation between SIC and the wind stress curl or the SAM index, but the reason remains to be explored.

5. Conclusions

This study focuses on the wCSP event formed at the end of June and maintained until mid-July in 2009. The Southern Ocean State Estimate is used to analyze the heat budget and the underlying physical processes controlling the evolution of the polynya. Negative wind stress curl from

cyclonic atmospheric circulations induces upwelling of warm CDW to the surface. Cyclones create differences in the meridional velocities across the northern and southern boundaries of the polynya, and lead to net meridional heat transport into the polynya. The two processes contribute to the formation of the embayment — the precursor of the polynya. The cyclonic wind field also promotes the convergence of sea ice over the northern portion of the embayment, finally leading to the formation of the polynya. A negative relationship between SIC and SAM was found, although the mechanisms need to be explored. The existence of wCSP in the winter potentially has an impact on the phytoplankton production in spring.

This study emphasizes the role of horizontal advection as a heat source for the formation and maintenance of an open-ocean polynya, while previous studies addressed the role of vertical heat flux associated with the upwelling of warm water. The relationship between the occurrence of the wCSP is elucidated, although the role of cyclones in building such a relationship needs to be confirmed by using cyclone-tracking techniques (e.g., Uotila et al., 2013). In the coming decades, SAM may continue a trend toward more positive values (Zheng et al., 2013), and may result in more cyclones in high-latitudes of the Southern Ocean, which may affect the formation of wCSP. This is worth exploring by future work.

Author statement

Zheng Wei: Methodology, Writing-Original draft, Formal analysis, Software.

Zhaoru Zhang: Conceptualization, Supervision, Funding acquisition, Writing-Reviewing and Editing.

Xiaoqiao Wang: Software, Writing-Reviewing and Editing.

Yuanjie Chen: Software.

Meng Zhou: Resources, Supervision, Funding acquisition.

Declaration of competing interest

The authors declare that they have no known competing financial interests or personal relationships that could have appeared to influence the work reported in this paper.

Acknowledgements

This work is funded by the Impact and Response of Antarctic Seas to Climate Change (Grant 583 No: IRASCC 1-02-01B), the Shanghai Science and Technology Committee (Grant No. 20230711100 and Grant No. 21QA1404300), the National Natural Science Foundation of China (Grant No. 41876221 and 41941008), the National Key Research and Development Program of China (Grant No. 2019YFC1509102) and the Advanced Polar Science Institute of Shanghai (APSIS). The SOSE solution for years 2005–2010 is available from sose.ucsd.edu. The satellite data used for model validation are available from the NASA National Snow and Ice Data Center (NSIDC) (https://nsidc.org/). The *in situ* observation data used for model validation is available from the BROKE-West voyage (https://data.aad.gov.au/metadata/records/200506030).

References

Abernathey, R.P., Cerovecki, I., Holland, P.R., Newsom, E., Mazloff, M., Talley, L.D., 2016. Water-mass transformation by sea ice in the upper branch of the Southern Ocean overturning. Nat. Geosci. 9, 596–601. https://doi.org/10.1038/ngeo2749.

Arbetter, T.E., Lynch, A.H., Bailey, D.A., 2004. Relationship between synoptic forcing and polynya formation in the Cosmonaut Sea: 1. Polynya climatology. J. Geophys. Res. Oceans 109. https://doi.org/10.1029/2003JC001837.

Arrigo, K.R., Robinson, D.H., Worthen, D.L., Dunbar, R.B., DiTullio, G.R., VanWoert, M., Lizotte, M.P., 1999. Phytoplankton community structure and the drawdown of nutrients and CO_2 in the Southern Ocean. Science 283, 365–367. https://doi.org/10.1126/science.283.5400.365.

Bailey, D.A., Lynch, A.H., Arbetter, T.E., 2004. Relationship between synoptic forcing and polynya formation in the Cosmonaut Sea: 2. Regional climate model simulations. J. Geophys. Res. Oceans 109. https://doi.org/10.1029/2003JC001838.

Berg, L., Prend, C.J., Campbell, E.C., Mazloff, M.R., Talley, L.D., Gille, S.T., 2020. Weddell Sea phytoplankton blooms modulated by sea ice variability and polynya formation. Geophys. Res. Lett. 47, 1–10. https://doi.org/10.1029/2020GL087954.

Boyd, P.W., Jickells, T., Law, C.S., Blain, S., Boyle, E.A., Buesseler, K.O., Coale, K.H., Cullen, J.J., De Baar, H.J.W., Follows, M., Harvey, M., Lancelot, C., Levasseur, M., Owens, N.P.J., Pollard, R., Rivkin, R.B., Sarmiento, J., Schoemann, V., Smetacek, V., Takeda, S., Tsuda, A., Turner, S., Watson, A.J., 2007. Mesoscale iron enrichment experiments 1993-2005: synthesis and future directions. Science 315, 612–617. https://doi.org/10.1126/science.1131669.

Campbell, E.C., Wilson, E.A., Moore, G.W.K., Riser, S.C., Brayton, C.E., Mazloff, M.R., Talley, L.D., 2019. Antarctic offshore polynyas linked to Southern Hemisphere climate anomalies. Nature 570, 319–325. https://doi.org/10.1038/s41586-019-1294-0.

Cheon, W.G., Park, Y.G., Toggweiler, J.R., Lee, S.K., 2014. The relationship of Weddell Polynya and open-ocean deep convection to the Southern Hemisphere westerlies. J. Phys. Oceanogr. 44, 694–713. https://doi.org/10.1175/JPO-D-13-0112.1.

Comiso, J.C., Gordon, A.L., 1987. Recurring polynyas over the Cosmonaut Sea and the Maud Rise. J. Geophys. Res. Oceans 92, 2819–2833. https://doi.org/10.1029/JC092iC03p02819.

Comiso, J.C., Gordon, A.L., 1996. Cosmonaut polynya in the Southern Ocean: structure and variability. J. Geophys. Res. Oceans 101, 18297–18313. https://doi.org/10.1029/96JC01500.

De Baar, H.J.W., Boyd, P.W., Coale, K.H., Landry, M.R., Tsuda, A., Assmy, P., Bakker, D. C.E., Bozec, Y., Barber, R.T., Brzezinski, M.A., Buesseler, K.O., Boyé, M., Croot, P.L., Gervais, F., Gorbunov, M.Y., Harrison, P.J., Hiscock, W.T., Laan, P., Lancelot, C., Law, C.S., Levasseur, M., Marchetti, A., Millero, F.J., Nishioka, J., Nojiri, Y., van Oijen, T., Riebesell, U., Rijkenberg, M.J.A., Saito, H., Takeda, S., Timmermans, K.R., Veldhuis, M.J.W., Waite, A.M., Wong, C.S., 2005. Synthesis of iron fertilization experiments: from the iron age in the age of enlightenment. J. Geophys. Res. Oceans 110, 1–24. https://doi.org/10.1029/2004JC002601.

Ding, Y., Cheng, X., Li, X., Shokr, M., Yuan, J., Yang, Q., Hui, F., 2020. Specific relationship between the surface air temperature and the area of the Terra Nova Bay Polynya, Antarctica. Adv. Atmos. Sci. 37, 532–544. https://doi.org/10.1007/s00376-020-9146-2.

Fenty, I., Heimbach, P., 2013. Coupled sea ice–ocean-state estimation in the Labrador Sea and Baffin Bay. J. Phys. Oceanogr. 43, 884–904. https://doi.org/10.1175/JPO-D-12-065.1.

Forget, G., 2010. Mapping ocean observations in a dynamical framework: a 2004-06 ocean atlas. J. Phys. Oceanogr. 40, 1201–1221. https://doi.org/10.1175/2009JPO4043.1.

Francis, D., Eayrs, C., Cuesta, J., Holland, D., 2019. Polar cyclones at the origin of the reoccurrence of the Maud Rise Polynya in austral winter 2017. J. Geophys. Res. Atmos. 124, 5251–5267. https://doi.org/10.1029/2019jd030618.

Geddes, J.A., Moore, G.W.K., 2007. A climatology of sea ice embayments in the Cosmonaut Sea, Antarctica. Geophys. Res. Lett. 34, 2–6. https://doi.org/10.1029/2006GL027910.

Gille, S.T., McKee, D.C., Martinson, D.G., 2016. Temporal changes in the Antarctic circumpolar current: Implications for the Antarctic continental shelves. Oceanography 29, 96–105. https://doi.org/10.5670/oceanog.2016.102.

Gordon, A.L., 2014. Oceanography: southern Ocean polynya. Nat. Clim. Change 4, 249–250. https://doi.org/10.1038/nclimate2179.

Gordon, A.L., Visbeck, M., Comiso, J.C., 2007. A possible link between the Weddell Polynya and the southern annular mode. J. Clim. 20, 2558–2571. https://doi.org/10.1175/JCLI4046.1.

Guo, G., Shi, J., Gao, L., Tamura, T., Williams, G.D., 2019. Reduced sea ice production due to upwelled oceanic heat flux in Prydz Bay, East Antarctica. Geophys. Res. Lett. 46, 4782–4789. https://doi.org/10.1029/2018GL081463.

Haid, V., Timmermann, R., 2013. Simulated heat flux and sea ice production at coastal polynyas in the southwestern Weddell Sea. J. Geophys. Res. Oceans 118, 2640–2652. https://doi.org/10.1002/jgrc.20133.

Hersbach, H., Bell, B., Berrisford, P., et al., 2020. The ERA5 global reanalysis. Q. J. Roy. Meteorol. Soc. 146, 1999–2049. https://doi.org/10.1002/qj.3803, 2020.

Hibler III, W.D., 1979. A dynamic thermodynamic sea ice model. J. Phys. Oceanogr. 9, 815–846. https://doi.org/10.1175/1520-0485(1979)0092.0.CO;2.

Hirabara, M., Tsujino, H., Nakano, H., Yamanaka, G., 2012. Formation mechanism of the Weddell Sea Polynya and the impact on the global abyssal ocean. J. Oceanogr. 68, 771–796. https://doi.org/10.1007/s10872-012-0139-3.

Hoppema, M., Anderson, L.G., 2007. Chapter 6. Biogeochemistry of polynyas and their role in sequestration of anthropogenic constituents. Elsevier Oceanogr. Ser. 74, 193–221. https://doi.org/10.1016/S0422-9894(06)74006-5.

Jena, B., Pillai, A.N., 2020. Satellite observations of new phytoplankton blooms in the Maud Rise Polynya. Southern Ocean. Cryosph. Discuss. 14, 1385–1398. https://doi.org/10.5194/tc-2019-282.

Kurihara, Y., 1965. On the use of implicit and iterative methods for the time integration of the wave equation. Mon. Weather Rev. 93, 33–46. https://doi.org/10.1175/1520-0493(1965)093<0033:OTUOIA>2.3.CO;2.

Lei, R.B., Gui, D.W., Yuan, Z.L., Pang, X.P., Tao, D., Zhai, M.X., 2020. Characterization of the unprecedented polynya events north of Greenland in 2017/2018 using remote sensing and reanalysis data. Acta Oceanol. Sin. 39, 5–17. https://doi.org/10.1007/s13131-020-1643-8.

Marshall, G.J., 2003. Trends in the southern annular mode from observations and reanalyses. J. Clim. 16, 4134–4143. https://doi.org/10.1175/1520-0442(2003)016<4134:TITSAM>2.0.CO;2.

Mazloff, M.R., Heimbach, P., Wunsch, C., 2010. An eddy-permitting Southern Ocean state estimate. J. Phys. Oceanogr. 40, 880–899. https://doi.org/10.1175/2009JPO4236.1.

Morales Maqueda, M.A., Willmott, A.J., Biggs, N.R.T., 2004. Polynya dynamics: a review of observations and modeling. Rev. Geophys. 42 https://doi.org/10.1029/2002RG000116.

Mundy, C.J., Barber, D.G., 2001. On the relationship between spatial patterns of sea-ice type and the mechanisms which create and maintain the North Water (NOW) polynya. Atmos.-Ocean 39, 327–341. https://doi.org/10.1080/07055900.2001.9649684.

Prasad, T.G., McClean, J.L., Hunke, E.C., Semtner, A.J., Ivanova, D., 2005. A numerical study of the western Cosmonaut polynya in a coupled ocean-sea ice model. J. Geophys. Res. Oceans 110, 1–21. https://doi.org/10.1029/2004JC002858.

Semtner, A.J., 1976. A model for the thermodynamic growth of sea ice in numerical investigations of climate. J. Phys. Oceanogr. 6, 379–389. https://doi.org/10.1175/1520-0485(1976)0062.0.CO;2.

Sen Gupta, A., England, M.H., 2006. Coupled ocean–atmosphere–ice response to variations in the Southern Annular Mode. J. Clim. 19, 4457–4486. https://doi.org/10.1175/JCLI3843.1.

Simpkins, G.R., Karpechko, A.Y., 2011. Sensitivity of the southern annular mode to greenhouse gas emission scenarios. Clim. Dynam. 38, 563–572. https://doi.org/10.1007/s00382-011-1121-2.

Uotila, P., Vihma, T., Tsukernik, M., 2013. Close interactions between the Antarctic cyclone budget and large-scale atmospheric circulation. Geophys. Res. Lett. 40, 3237–3241. https://doi.org/10.1002/grl.50560.

White, W.B., Peterson, R.G., 1996. An Antarctic circumpolar wave in surface pressure, wind, temperature and sea-ice extent. Nature 380, 699–702. https://doi.org/10.1038/380699a0.

Zheng, F., Li, J., Clark, R.T., Nnamchi, H.C., 2013. Simulation and projection of the Southern Hemisphere annular mode in CMIP5 models. J. Clim. 26, 9860–9879. https://doi.org/10.1175/JCLI-D-13-00204.1.